ЖЭТФ, 2003, том 123, вып. 3, стр. 518–526 © 2003

MEASUREMENT OF THE TEMPERATURE DEPENDENCE OF THE $dd\mu$ MOLECULE FORMATION RATE IN DENSE DEUTERIUM AT TEMPERATURES 85–790 K

V. R. Bom [a], ***D. L. Demin*** [b], ***C. W. E. van Eijk*** [a], ***V. V. Filchenkov*** [b], ***N. N. Grafov*** [b]*, ***V. G. Grebinnik*** [b], ***K. I. Gritsaj*** [b], ***A. D. Konin*** [b], ***A. V. Kuryakin*** [c], ***V. A. Nazarov*** [c], ***V. V. Perevozchikov*** [c], ***A. I. Rudenko*** [b], ***S. M. Sadetsky*** [d], ***Yu. I. Vinogradov*** [c], ***A. A. Yukhimchuk*** [c], ***S. A. Yukhimchuk*** [b], ***V. G. Zinov*** [b], ***S. V. Zlatoustovskii*** [c]

[a] *Delft University of Technology*
2629 JB Delft, the Netherlands

[b] *Joint Institute for Nuclear Research, Dzhelepov Laboratory of Nuclear Problems*
141980, Dubna, Moscow Region, Russia

[c] *Russian Federal Nuclear Center, All-Russian Research Institute of Experimental Physics*
607200, Sarov, Nizhny Novgorod Region, Russia

[d] *St. Petersburg Nuclear Physics Institute*
188350, Gatchina, Leningrad Region, Russia

Submitted 29 July 2002

Muon catalyzed fusion (MCF) in deuterium was studied by the MCF collaboration at the Joint Institute for Nuclear Research phasotron. The measurements were carried out with a high-pressure deuterium target in the temperature range 85–790 K at densities about 0.5 and 0.8 of the liquid hydrogen density. The first experimental results for the $dd\mu$ molecule formation rate $\lambda_{dd\mu}$ in the temperature range 400–790 K with deuterium density about 0.5 of the liquid hydrogen density are presented.

PACS: 36.10.-k, 36.10.Dr

1. MOTIVATION

The processes of muon catalyzed fusion (MCF) in deuterium were studied in many laboratories [1–10]. Recent years have seen significant success both in theoretical consideration [11–14] and in the measurements of the $dd\mu$ molecule formation rate including strong spin effects. Recent data [9, 10] give an example of the progress achieved in the accuracy of measuring the fine effects of MCF in low-density deuterium gas at temperatures 28–350 K. But there are still no direct experimental data for the MCF processes at temperatures above 400 K. The only experimental (nondirect) result for $\lambda_{dd\mu}$ at temperatures up to 600 K [2] was obtained from the analysis of muon losses in the experiment with double deuterium–tritium mixtures and had big errors. It is important that at these temperatures, a large $dd\mu$ formation rate for the $d\mu$ atom spin state $F = 1/2$ should be expected to prevail over that for the spin $F = 3/2$ [14]. These measurements of $\lambda_{dd\mu}$ at high temperatures are also necessary for correcting the evaluation of the parameters of the dt fusion cycle derived from the experiments [15].

Here, we present the results of the measurements in a dense deuterium gas in a wide temperature range 85–790 K. The aim of the experiment was to measure the formation rate $\lambda_{dd\mu}$ in dense deuterium for the first time in the temperature range up to 800 K. The scheme of the process is presented in Fig. 1.

*E-mail: grafov@nu.jinr.ru

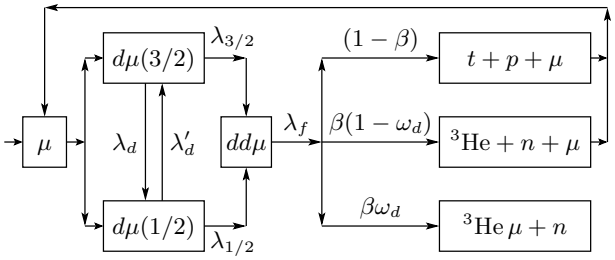

Fig. 1. Scheme of the dd cycle

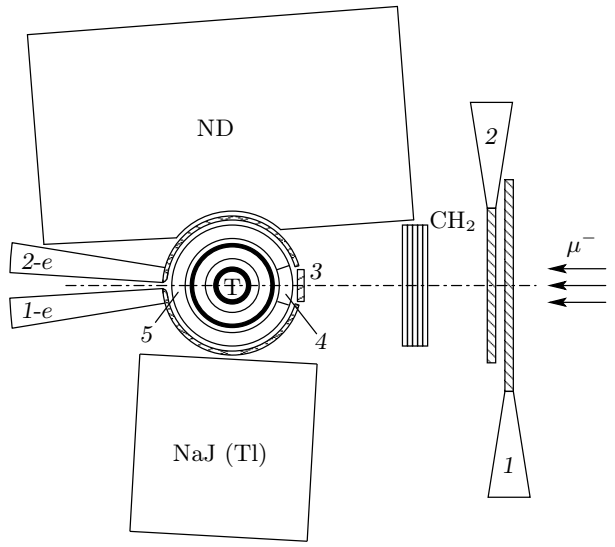

Fig. 2. Experimental layout

2. EXPERIMENT

The experimental method is similar to that used in [16]. We measured and analyzed the time and charge (deposited energy in a neutron detector) distributions of 2.5 MeV neutrons from the dd fusion reactions

$$d\mu + d \to dd\mu \to {}^3\mathrm{He} + n + \mu, \qquad (1)$$

$$d\mu + d \to dd\mu \to {}^3\mathrm{He}\mu + n. \qquad (2)$$

The simplified experimental layout is shown in Fig. 2. The essence of the experimental installation is described in [17]. The installation was mounted on the muon beam line of the Joint Institute for Nuclear Research phasotron.

2.1. Target

The central part of the installation is a specially constructed deuterium high-pressure target (T) [18] of

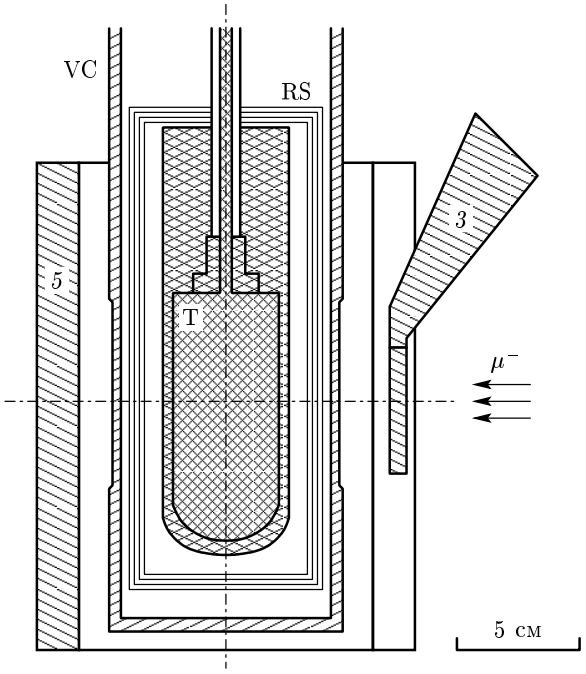

Fig. 3. Scheme of the deuterium high-pressure target. RS are radiation screens, VC is the vacuum chamber, 3 and 5 are scintillation counters depicted in Fig. 2

the volume 76 cm^3 (Fig. 3). The ampoule of the target is made with the special hydrogen-resistant alloy XH40MDTYu-ID. The ampoule is surrounded by a set of radiation screens (RS) and is placed inside the vacuum chamber (VC) made with stainless steel. The total amount of wall matter on the muon beam path is about 11 mm. The target is able to withstand pressures up to 1500 bar at temperatures up to 800 K. A set of devices [18] was used for handling the deuterium gas. To achieve the deuterium purity of impurities with $Z > 1$ at a level of 0.1 *ppm*, the target was filled using a palladium filter and a vanadium–deuterium pressure source [19].

2.2. Detectors

The target is surrounded by a set of detectors. Scintillation counters 1–3 detected incoming muons. Cylinder-shaped scintillation counters *4* and *5* served to select muon stops in the target (signal $1 \cdot 2 \cdot 3 \cdot 4 \cdot \bar{5}$). Specially designed cylinder-shaped scintillation counters 1-e and 2-e were used to detect μ-decay electrons. A coincidence between the signals of counters 5 and 1-e, 2-e was considered as a μ-decay electron. A large neutron detector (with the NE-213 volume 12.5 l) [20] was aimed to detect neutrons from reactions (1) and (2). To

reduce the background, the n–γ separation was realized by comparing signals for the total light and the fast component light of the neutron detector signal. The γ-quantum discrimination efficiency was better than 10^{-3} for energies larger than 100 keV.

The NaI(Tl) crystal was used to search for the rare fusion channel $d(d,\gamma)^4$He in parallel to the main aim of the experiment (the subject matter of this paper).

The timing sequence of the 4, 5, 1-e, 2-e, and neutron detector signals was registered by flash ADC and was recorded on a PC. The trigger is described in [22].

2.3. Experimental conditions

Two exposure runs were carried out. One was with the target filled with an equilibrium protium–deuterium mixture (21 % of H) in the temperature range 85–300 K at the density $\varphi \approx 0.84$ LHD (as usual, density is given in units of the liquid hydrogen density, LHD $= 4.25 \cdot 10^{22}$ nucl/cm^3). The exposure at $\varphi \approx 0.47$ LHD was also measured at the temperature 300 K.

The other exposure run was carried out with the target filled with pure deuterium (protium content was about 0.1 %) in the temperature range 300–790 K at the density $\varphi \approx 0.48$ LHD.

The experimental conditions and the gathered electron statistics for all runs are presented in Table 1. The background exposure with an empty target was also carried out.

3. KINETICS OF THE $dd\mu$ FUSION CYCLE

The basic processes of the kinetics of the resonant formation of $dd\mu$ molecules are considered in [11, 12]. The $d\mu$ atoms are formed during the time about $10^{-12} \cdot \varphi^{-1}$ s [23] with the energy of a few eV and are thermalized with the rate about $10^9 \cdot \varphi$ s^{-1} [24]. Two different hyperfine states of the $d\mu$ atoms $F = 3/2$ and $F = 1/2$ are statistically populated with the respective probabilities 2/3 and 1/3. After that, processes of resonant $dd\mu$ formation (3) and $d\mu$ atom spin-flip processes (4) occur,

$$d\mu + D_2 \to [(dd\mu)dee]^*, \tag{3}$$

$$(d\mu)_{F=3/2} + \mathrm{D}_2 \leftrightarrow (d\mu)_{F=1/2} + \mathrm{D}_2. \tag{4}$$

The rates of direct and inverse spin-flip processes (4) (λ_d and λ'_d) are connected by the detailed balance relation

$$\begin{gathered}\lambda'_d = \gamma\lambda_d, \quad \gamma = 2\exp(-\Delta E/T), \\ \Delta E = 0.0485\,\text{eV}.\end{gathered} \tag{5}$$

In the process of resonant $dd\mu$ formation (3), the released energy (the binding energy of the formed $dd\mu$ mesomolecule) is transmitted to the excitation of vibration-rotational states of the mesic molecular complex $[(dd\mu)dee]^*$. In the case of the usually nonresonant $dd\mu$ formation,

$$d\mu + \mathrm{D}_2 \to [(dd\mu)de]^+ + e, \tag{6}$$

the released energy is taken away by a conversion electron. The rate of this nonresonant mechanism (λ_{nr}) is sufficiently small and increases with the temperature (energy) as [25]

$$\begin{gathered}\lambda_{nr} = \lambda_1 + \lambda_2(3/2)kT, \quad \lambda_1 = 0.04\,\mu\text{s}^{-1}, \\ \lambda_2 = 2.3\,\mu\text{s}^{-1}\cdot\text{eV}^{-1}.\end{gathered} \tag{7}$$

In the formed $dd\mu$ complex (3), the processes of dd fusion (with rates $\lambda_f \sim 10^9$ s^{-1} [26])

$$dd\mu \to {}^3\mathrm{He} + n + \mu, \tag{8}$$

$$dd\mu \to t + p + \mu, \tag{9}$$

$$dd\mu \to {}^3\mathrm{He}\mu + n \tag{10}$$

compete with the processes of complex deexitation and complex back decay. The $d\mu$ atom formation rate and the thermalization rate as well as the dd fusion rate are much higher than the effective hyperfine transition rates and the effective (experimentally observable) mesomolecule formation rate. At times larger than the lifetime (~ 0.5 ns) of the mesomolecular complex, the kinetics is therefore described by the scheme in Fig. 1 and depends on the effective rates of spin-flip processes (4) and the effective rates of $dd\mu$ formation from two hyperfine states ($\lambda_{1/2}$ and $\lambda_{3/2}$). The following system of differential equations corresponds to the kinetics in Fig. 1 [11, 27]:

$$\begin{aligned}\frac{dN_{3/2}}{dt} = &-(\lambda_0+\lambda_d+\lambda_{3/2})N_{3/2}+\frac{2}{3}(1-w)\lambda_{3/2}N_{3/2}+ \\ &+\left[\frac{2}{3}(1-w)\lambda_{1/2}+\lambda_d{}'\right]N_{1/2},\end{aligned} \tag{11}$$

$$\begin{aligned}\frac{dN_{1/2}}{dt} = &-(\lambda_0+\lambda_d{}'+\lambda_{1/2})N_{1/2}+\frac{1}{3}(1-w)\lambda_{1/2}N_{1/2}+ \\ &+\left[\frac{1}{3}(1-w)\lambda_{3/2}+\lambda_d\right]N_{3/2},\end{aligned} \tag{12}$$

Table 1. Experimental conditions and statistics

Run	T, K	Content, %		φ, LHD	N_e
		H	D		
1	85 (1)	20.7 (0.1)	79.3 (0.5)	0.840 (0.025)	685 200
2	110 (1)	20.7 (0.1)	79.3 (0.5)	0.841 (0.025)	456 500
3	230 (1)	20.7 (0.1)	79.3 (0.5)	0.831 (0.025)	415 900
4	301 (3)	20.7 (0.1)	79.3 (0.5)	0.831 (0.025)	427 000
5	299 (3)	20.7 (0.1)	79.3 (0.5)	0.473 (0.014)	374 900
6	290 (4)	0.1 (0.1)	99.9 (0.1)	0.480 (0.014)	355 500
7	401 (10)	0.1 (0.1)	99.9 (0.1)	0.480 (0.014)	226 900
8	530 (10)	0.1 (0.1)	99.9 (0.1)	0.480 (0.014)	194 900
9	660 (10)	0.1 (0.1)	99.9 (0.1)	0.480 (0.014)	208 700
10	791 (15)	0.1 (0.1)	99.9 (0.1)	0.483 (0.020)	301 900

$$\frac{dN_n}{dt} = \beta\varphi(\lambda_{3/2}N_{3/2} + \lambda_{1/2}N_{1/2}). \qquad (13)$$

Here, $N_{3/2}$ and $N_{1/2}$ are populations of the $F = 3/2$ and $F = 1/2$ $d\mu$ atom hyperfine states, N_n is the number of fusion neutrons, $w = \beta w_d$, β is the probability of ^{3}He-reaction channel (8) and (10), $w_d = 0.13$ is the probability of muon sticking to ^{3}He [11], and λ_0 is the muon decay rate.

This system of differential equations (11)–(13) was considered and its approximate solution was obtained [11, 27].

4. ANALYSIS

The first step of the analysis of registered events consists in separation of neutrons, γ-quanta, and μ-decay electrons. For each exposure, we then build and analyze the time and charge (deposited energy in a neutron detector) distributions of fusion neutrons and the time distributions of μ-decay electrons.

4.1. Electron time spectra

Time spectra of electrons from muons stopped and decayed in the target were created and analyzed for each exposure including the background run with an empty target. Fitting the background electron time spectra from muons stopped and decayed in target walls allows us to obtain the form of this distribution $B_{empty}(t)$. For each exposure with the deuterium filled target, we then fitted the electron time spectra, with the obtained form of the background spectra taken into account using the formula

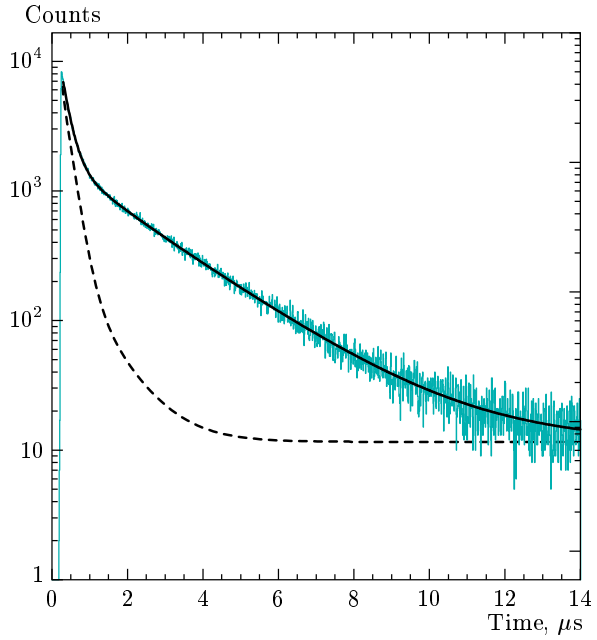

Fig. 4. Example of the experimental time spectrum of electrons from μ decay. Solid line is the fitting function. Dashed line corresponds to the empty target

$$N_e^{total}(t) = kB_{empty}(t) + A_e \exp(-\lambda_e t) + F,$$

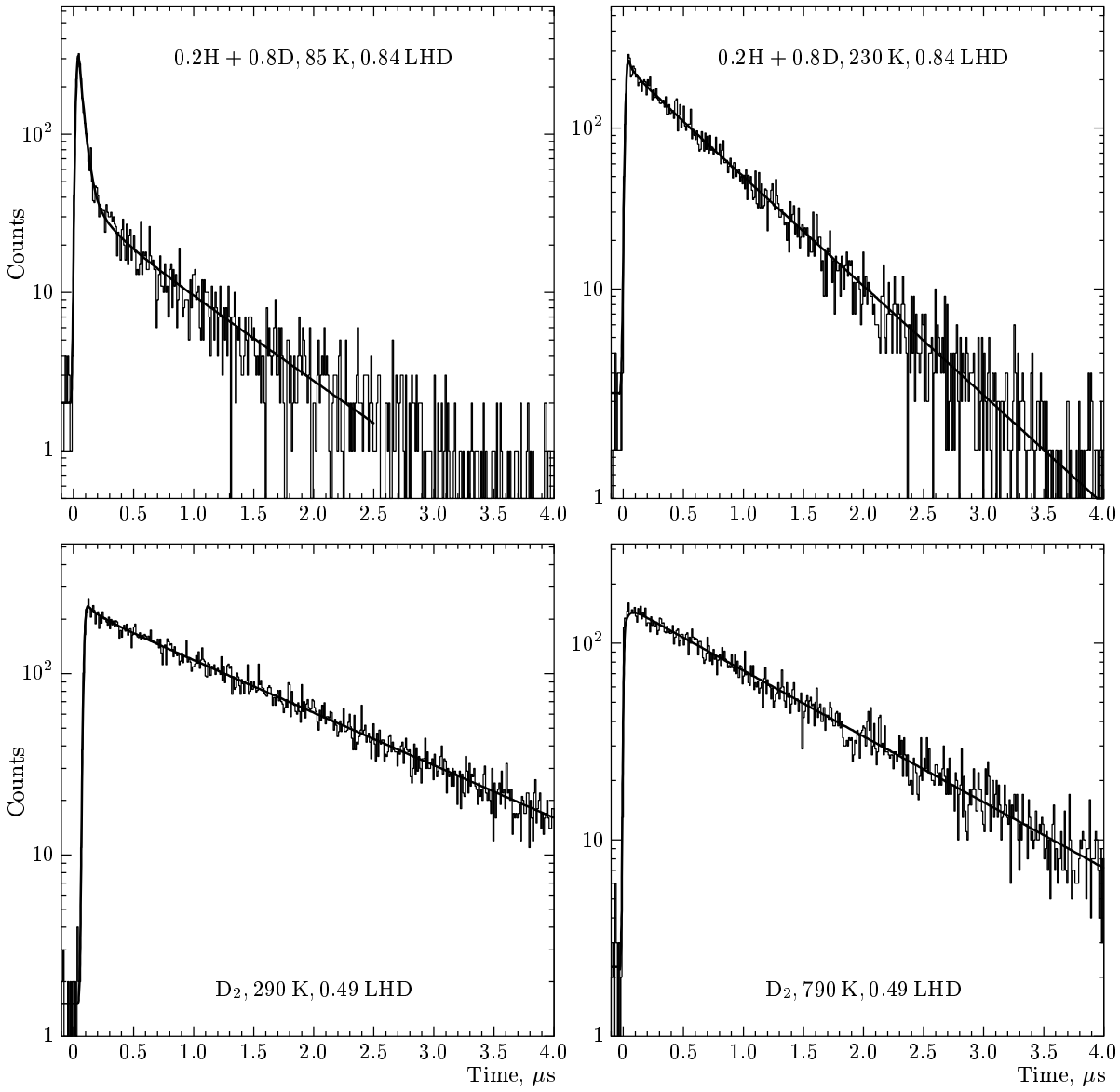

Fig. 5. Experimental time spectra of fusion neutrons measured for exposures at the temperatures 85, 230, 290, and 790 K. Solid lines are the fitting functions

where λ_e is the muon disappearance rate and F is an accidental background. In this fit, k, A_e, λ_e, and F are parameters. As a result, the numbers of electrons $N_e = A_e/\lambda_e$ from the muons stopped in deuterium were obtained. The numbers N_e were necessary for normalization. A typical example of the fitted time distributions of decay electrons for the deuterium-filled target is shown in Fig. 4. The dashed line corresponds to the electrons from decays of muons stopped in the target walls (empty target).

The observed muon disappearance rates λ_e are in agreement with the muon decay rate $\lambda_0 = 0.455\,\mu\text{s}^{-1}$ with an accuracy not worse than 1.5 %. The analysis of electron time distributions showed that about 45 % of all the incoming muons stop in deuterium. The rest part of muons stops in target walls.

4.2. Neutron time and charge spectra

Only the first detected neutrons were selected for the analysis. To reduce the background, we used the time selection criterion [28]

$$t_n + 0.5\,\mu\text{s} < t_e < t_n + 4.5\,\mu\text{s}, \qquad (14)$$

where t_n and t_e are neutron and electron detection times measured from the moment of muon stop in the target. The time and charge (energy) distributions were plotted for these events. Examples of time distributions of fusion neutrons are shown in Fig. 5 for four temperatures.

According to [11, 27], the solution of the system of differential equations (11)–(13), the time distributions of the first neutrons detected with the efficiency ϵ, is given by the sum of two exponentials,

$$N_n(t) = A_{fast}\exp(-\lambda_{fast}t) + \\ + A_{slow}\exp(-\lambda_{slow}t). \quad (15)$$

The parameters of this expression are functions of λ_d, $\lambda_{1/2}$, $\lambda_{3/2}$, and $\alpha \equiv \epsilon + \omega - \epsilon\omega$. They can be reconstructed from the amplitudes and slopes of the exponentials in (15). The amplitude A_{fast} of the first term in (15) is related to the $dd\mu$ formation from the $d\mu$ atom with the spin $F = 3/2$ and the corresponding slope λ_{fast} is determined mainly by the value of λ_d. The amplitude of the second term (slow component) corresponds to the so-called steady state of the $dd\mu$ cycle. The steady state $dd\mu$ formation rate $\lambda^{ss}_{dd\mu}$ presents the «mean» value of the $dd\mu$ formation rate from different $d\mu$ spin states for times $t > \lambda^{-1}_{fast}$. The ratio of the amplitudes A_{fast}/A_{slow} is responsible for the ratio $\lambda_{3/2}/\lambda_{1/2}$.

The values of $\lambda^{ss}_{dd\mu}$ were obtained from

$$\lambda^{ss}_{dd\mu} = \frac{\lambda_n}{\varphi\beta}\,\frac{N_n}{N_e\epsilon f_t}. \quad (16)$$

Here, the second ratio gives the absolute neutron yield for the steady state of the dd cycle, λ_n is the slow exponent slope of (15), and N_n is the number of fusion neutrons. The time selection factor $f_t = 0.67$ is due to criterion (14).

Determination of the neutron detection efficiency ϵ is analogous to that in [29]. To determine the efficiency loss due to a finite energy threshold, the calculated recoil proton energy spectrum was reconciled with the experimental energy distribution. This procedure was done for each exposure, its example is given in Fig. 6. The line in the figure is the calculated response function of the neutron detector and the histogram is the experimental energy distribution. The efficiency of the neutron detector is obtained to be approximately 12 % and its accuracy is about 8 %.

The fit strategy was as follows. At the first step, we fitted only the slow part of the neutron time spectra and found the steady state formation rates ($\lambda^{ss}_{dd\mu}$) using expression (16). At the next step, we fitted the entire neutron time spectra using formula (15). In this fit, formula (15) was convolved with a Gaussian resolution function to allow for a finite time resolution and to determine the time zero position. The analysis showed that the time zero stability during data taking was better than 1 ns. The background due to muon stops in the target walls and due to accidental coincidence was taken into account in the fit procedure. At the final step of the analysis, the values of $\lambda_{3/2}$, $\lambda_{1/2}$, and λ_d were obtained from the values of $\lambda^{ss}_{dd\mu}$ and parameters of expression (15). The method developed in [27] was used for this purpose.

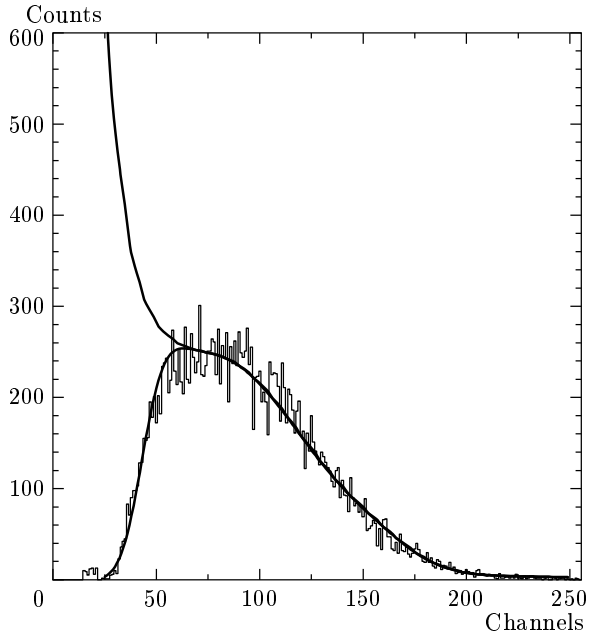

Fig. 6. Neutron energy distribution. The histogram is the experimental neutron energy distribution. The solid line is the calculated response function of the neutron detector

We made some corrections to the final values of the rates that are due to the nonresonant $dd\mu$ formation rate on molecules D_2 and HD [30] (in runs with double H/D mixtures).

It turned out that a reliable separation of fast and slow terms of (15) in fitting is possible only at low temperatures (in our case, not higher than 290 K), where the rates $\lambda_{3/2}$ and $\lambda_{1/2}$ are essentially different and λ_d is much larger than λ'_d. At high temperatures (higher than 300 K), the rates $\lambda_{3/2}$ and $\lambda_{1/2}$ are approximately equal [14], and it is therefore a great problem in fitting to obtain the fast component parameters and thus to distinguish the values of $\lambda_{3/2}$ and $\lambda_{1/2}$. At these temperatures, we obtained only the value of $\lambda^{ss}_{dd\mu}$. For

λ_d, which is determined from the fast exponent slope, we obtained its value only at the temperatures 85 and 110 K for the same reasons.

5. RESULTS AND DISCUSSIONS

The obtained values of $\lambda^{ss}_{dd\mu}$, λ_d, $\lambda_{3/2}$, and $\lambda_{1/2}$ are presented in Tables 2 and 3. All rates are normalized to the liquid hydrogen density. The statistic error is 2–3 %. The main sources of systematic errors are the uncertainties of the neutron detector efficiency (about 8 %) and gas density (about 3 %).

In Fig. 7, the temperature dependence $\lambda^{ss}_{dd\mu}(T)$ is shown together with the data [2]. The main result of this work is the direct measurement of the steady state $dd\mu$ formation rate at temperatures above 400 K. As can be seen, our data are in good agreement with theoretical predictions [14] at low temperatures (up to 400 K). But the experimental data are slightly larger than the theoretical ones at high temperatures.

In Fig. 8, the temperature dependence of $\lambda_{1/2}$ and $\lambda_{3/2}$ is shown. The solid line is theoretical calculations [14]. The values of λ_d, $\lambda_{1/2}$, and $\lambda_{3/2}$ are in good agreement with the theory and with other experimental data [9, 10, 17].

As mentioned above, reliably separating fast and slow terms in (15) in fitting, and hence obtaining the values of λ_d, $\lambda_{1/2}$, and $\lambda_{3/2}$ is possible only at low temperatures in our experimental conditions. The lifetime of the fast component of neutron spectra (15) is

$$\tau = \frac{1}{\lambda_{fast}} \sim \frac{1}{\lambda_d \varphi}.$$

Under our conditions ($\varphi \approx 0.5$ LHD), it approximately equals 50 ns, or about five channels in the measured time histogram. This fact is also confirmed by our Monte Carlo calculations. It is therefore worth to carry out an experiment at high temperatures with low-density deuterium (about 0.05 LHD), where the spin effect time range at neutron time distributions is about

Table 2. Experimental results for the steady state $dd\mu$ formation rate

T, K	$\lambda^{ss}_{dd\mu}$, μs^{-1}		
	Value	Stat. error	Syst. error
85	0.197	0.007	0.018
110	0.485	0.015	0.044
230	2.06	0.06	0.19
301	2.69	0.08	0.24
299	2.57	0.08	0.24
290	2.67	0.08	0.24
401	3.00	0.09	0.27
530	3.10	0.09	0.27
660	2.67	0.08	0.24
791	2.30	0.07	0.21

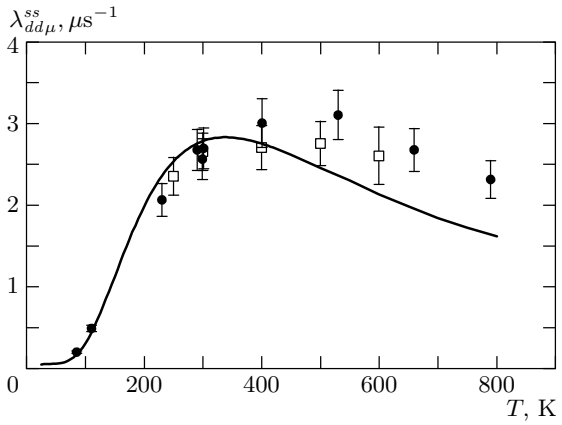

Fig. 7. Values of $\lambda^{ss}_{dd\mu}$ as a function of temperature. Circles are our data, squares are the LAMPF data [2]; the line is theory [14]

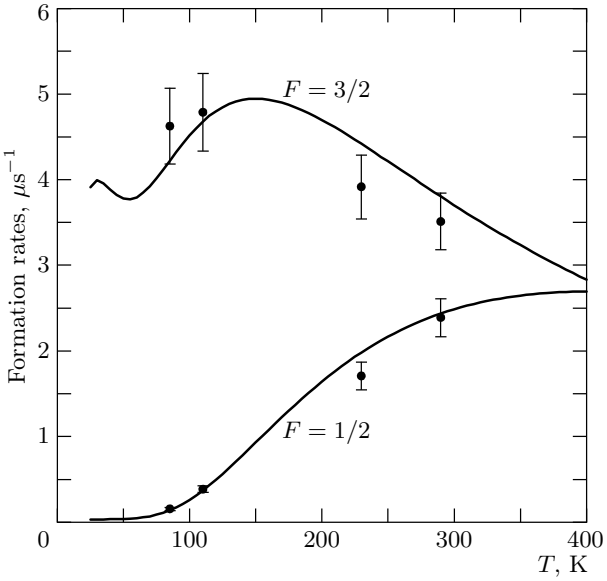

Fig. 8. Values of $\lambda_{3/2}$ and $\lambda_{1/2}$ as a function of temperature; the lines are the theory [14]

Table 3. Experimental results for the effective $dd\mu$ formation rates from different spin states and the effective $d\mu$ spin-flip rate

T, K	$\lambda_{1/2}$, μs^{-1}			$\lambda_{3/2}$, μs^{-1}			λ_d, μs^{-1}		
	Value	Stat. error	Syst. error	Value	Stat. error	Syst. error	Value	Stat. error	Syst. error
85	0.170	0.006	0.015	4.63	0.13	0.42	32.8	1.0	3.2
110	0.403	0.014	0.036	4.79	0.14	0.43	31.4	1.2	3.2
230	1.72	0.06	0.16	3.92	0.12	0.35	–	–	–
290	2.40	0.08	0.22	3.52	0.10	0.32	–	–	–

0.5 μs. An experiment of this type could be conducted at a muon factory.

6. CONCLUSIONS

The first direct measurements of the muon catalyzed dd fusion cycle parameters at high temperatures (up to 790 K) are carried out. The values of the steady state $dd\mu$ formation rate are obtained for the entire temperature range. Comparison with theory showed good agreement at low temperatures (up to 400 K) and some difference at high temperatures (above 400 K). At low temperatures, the values of the effective rates $\lambda_{3/2}$ and $\lambda_{1/2}$ are obtained; they are in agreement with the theory. Measuring these hyperfine parameters in the high-temperature range seems to require an experiment of a special type, i.e., at low deuterium density (about (0.01–0.05) LHD) with a high-intensity muon beam.

The authors are grateful to L. I. Ponomarev, M. P. Faifman, and N. I. Voropaev for the discussions. We also wish to thank M.M. Petrovsky, A. P. Kustov, and the staff of the RFNC-VNIIEF group for their help in tests and runs. The work was supported by the Ministry of Atomic Energy of the RF (project 6.25.19.19.99.969) and the Ministry of Science and Technology of the RF (project 103-7(00)-II) and the RFBR (project 01-02-16425).

REFERENCES

1. V. M. Bystritsky et al., Zh. Eksp. Teor. Fiz. **76**, 460 (1979).
2. S. E. Jones et al., Phys. Rev. Lett. **56**, 588 (1986).
3. D. V. Balin et al., Pis'ma Zh. Eksp. Teor. Fiz. **40**, 318 (1984).
4. D. V. Balin et al., Muon Cat. Fusion **2**, 241 (1988).
5. J. Zmeskal et al., Muon Cat. Fusion **1**, 109 (1987).
6. N. Nagele et al., Nucl. Phys. A **493**, 397 (1989).
7. V. M. Bystritsky et al., Muon Cat. Fusion **5/6**, 141 (1990/91).
8. D. V. Balin et al., Muon Cat. Fusion **5/6**, 163 (1990/91).
9. C. Petitjean, D. V. Balin, W. H. Breunlich et al., Hyp. Int. **118**, 127 (1999).
10. D. V. Balin et al., in *Proc. of the Conf.* $\mu CF-01$, Japan, Shimoda (2001).
11. M. P. Faifman et al., Zh. Exp. Teor. Fiz. **92**, 1173 (1987).
12. M. P. Faifman, Muon Cat. Fusion **2**, 247 (1988); M. P. Faifman, L. I. Menshikov, and T. A. Strizh, Muon Cat. Fusion **4**, 1 (1989).
13. A. Scrinzi, Muon Cat. Fusion **5/6**, 179 (1990).
14. M. P. Faifman, Hyp. Int. **101/102**, 179 (1996).
15. V. R. Bom et al., in *Proc. of the Conference* $\mu CF-01$, Japan, Shimoda (2001).
16. Yu. P. Averin et al., Hyp. Int. **118**, 111 (1999).
17. V. P. Dzhelepov et al., Zh. Eksp. Teor. Fiz. **101**, 1105 (1992); Muon Cat. Fusion **7**, 387 (1992).
18. V. V. Perevozchikov et al., Prib. Tekhn. Exp. **4**, 155 (2002); in *Proc. of the Conference* $\mu CF-01$, Japan, Shimoda (2001).

19. A. N. Golubkov and A. A. Yukhimchuk, in *Proc. of the Conference* $\mu CF-01$, Japan, Shimoda (2001); in *Proc. of the VII Int. Conf. Hydrogen Materials Science and Chemistry of Metal Hydrides*, ICHMS'2001, Alushta–Crimea–UKRAINE (2001), p. 298.

20. V. P. Dzhelepov et al., Nucl. Instr. and Meth. A **269**, 634 (1988).

21. L. N. Bogdanova et al., Preprint JINR E15-2001-264 (2001); Yad. Fiz. **65**, 1826 (2002).

22. V. G. Zinov, A. I. Rudenko, and V. T. Sidorov, Preprint JINR P13-96-439 (1996).

23. J. S. Cohen, Phys. Rev. A **27**, 167 (1983).

24. A. Adamchak and V. S. Melezhik, Muon Cat. Fusion **4**, 303 (1989).

25. S. I. Vinitsky et al., Zh. Eksp. Teor. Fiz. **74**, 849 (1978).

26. L. N. Bogdanova et al., Phys. Lett. B **115**, 171 (1982).

27. V. V. Filchenkov, Preprint JINR E1-89-57 (1989).

28. V. R. Bom et al., Zh. Eksp. Teor. Fiz. **84**(4), 641 (1997).

29. V. R. Bom and V. V. Filchenkov, Hyp. Int. **118**, 365 (1999).

30. G. G. Semenchuk et al., Hyp. Int. **118**, 141 (1999).